Full-Wave Modeling of Near-Field Radar Data for Planar Layered Media Reconstruction

Sébastien Lambot and Frédéric André

***Abstract*— A new near-field radar modeling approach for wave propagation in planar layered media is presented. The radar antennas are intrinsically modeled using an equivalent set of infinitesimal electric dipoles and characteristic, frequency-dependent, global reflection, and transmission coefficients. These coefficients determine through a plane wave decomposition wave propagation between the radar reference plane, point sources, and field points. The interactions between the antenna and layered medium are thereby inherently accounted for. The fields are calculated using 3-D Green's functions. We validated the model using an ultrawideband frequency-domain radar with a transmitting and receiving Vivaldi antenna operating in the range 0.8–4 GHz. The antenna characteristic coefficients are obtained from near- and far-field measurements over a copper plane. The proposed model provides unprecedented accuracy for describing near-field radar measurements collected over a water layer, the frequency-dependent electrical properties of which were described using the Debye model. Layer thicknesses could be retrieved through full-wave inversion. The proposed approach demonstrated great promise for nondestructive testing of planar materials and digital soil mapping using ground-penetrating radar.**

***Index Terms*— Antenna modeling, Green's functions, ground-penetrating radar (GPR), near-field, planar layered media.**

I. Introduction

NEAR-field radar techniques for nondestructive imaging and characterization of materials such as ground-penetrating radar (GPR) were subjected to intensive research for many years [1]–[3]. A major shortcoming in current knowledge is the modeling of the radar signal, which is necessary for quantitative reconstruction using inversion. Existing techniques usually rely strongly on simplifying assumptions, and in particular, neglect antenna effects, which include frequency-dependent radiation pattern, gain, phase delay, mutual coupling, and coupling with the medium of interest.

Antennas can be modeled using numerical approaches, such as the finite-difference time-domain (FDTD) method [4]–[7], the finite element method [8], [9], or the method of moments (MoM) [10], [11]. Yet, numerical approaches need significant computing resources and suffer from inherent differences between the real and conceptualized antenna models. For instance, Warren and Giannopoulos [5] used a 3-D FDTD approach through which the different parts of transmitting and receiving bowtie antennas were reproduced in the discretized model. Although relatively good modeling results were obtained for data collected over different emulsions, still significant modeling errors could be observed. Pantoja *et al.* [12] extended a MoM in the time domain for the transient analysis of thin-wire antennas located over a lossy half-space. Numerical analyses showed good results for cases where the antenna was not too close to a half-space medium.

More efficient techniques are based on electric field integral equation formulations [13]–[15], through which antennas are emulated using a set of infinitesimal electric dipoles and field points. The parameterization of these dipoles to properly describe real antenna radiation patterns is, however, not straightforward [14], [16]. In addition, such formulations do not directly account for wave propagation between the source or field points and the radar transmission line reference plane, and hence, antenna–medium interactions and mutual coupling are not directly accounted for. For instance, Gentili and Spagnolini [17] modeled a GPR horn antenna at some distance over a 3-D layered medium using an array of frequency-independent source dipoles and a feeding line characteristic impedance. Yet, with this approach the multiple reflections between the antenna terminal section and the medium were not accounted for.

For the particular case of far-field GPR with applications to planar layered media, Lambot *et al.* [18] proposed a closed-form, frequency-domain, radar equation that simultaneously accounts for: 1) all antenna effects through frequency-dependent global reflection and transmission coefficients and 2) wave propagation in layered media through 3-D Green's functions. This integrated antenna–medium model relies on the assumption that the spatial distribution of the backscattered field locally tends to a plane wave over the antenna aperture in far-field conditions. The model has demonstrated an unprecedented accuracy for describing radar data and retrieving medium electrical properties, including frequency dependence, in a series of hydrogeophysical and engineering applications [18]–[21]. In addition, the validity of that model being theoretically independent of frequency and antenna type, the approach also applies to electromagnetic induction (EMI). In that respect, Moghadas *et al.* [22] successfully applied this model to a loop antenna operating in the 30–60 kHz range for soil electrical conductivity determination. Whether for GPR or EMI, it was observed that the so-called far-field condition for the planar field approximation holds when the distance between the antenna and the medium is larger than the antenna aperture dimension.

Manuscript received March 9, 2012; revised December 19, 2012; accepted March 8, 2013. Date of publication May 27, 2013; date of current version February 27, 2014. This work was supported in part by the Fonds de la Recherche Scientifique, Belgium, and the DIGISOIL Project by the European Commission under the 7th Framework Programme for Research and Technological Development, Area "Environment," Activity 6.3 "Environmental Technologies."

The authors are with the Earth and Life Institute, Université Catholique de Louvain, Louvain-la-Neuve 1348, Belgium (e-mail: sebastien.lambot@uclouvain.be; frederic.andre@uclouvain.be).

Color versions of one or more of the figures in this paper are available online at http://ieeexplore.ieee.org.

Digital Object Identifier 10.1109/TGRS.2013.2259243

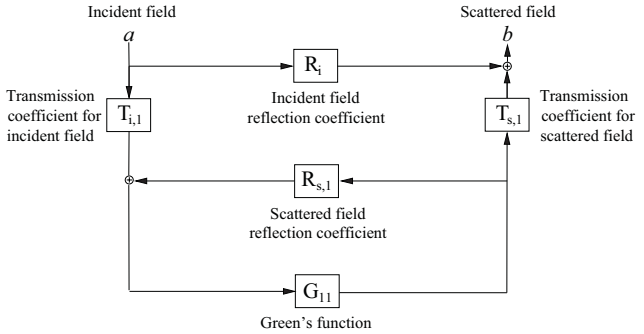

Fig. 1. Linear block diagram representing the far-field antenna model with global reflection and transmission coefficients that describe wave propagation between the radar reference plane and the source or field point [18].

In this paper, we generalize the far-field model of Lambot *et al.* [18] to near-field conditions. The radar antennas are modeled using an equivalent set of source and field points. The linear relations between the fields in the transmission line, the sources, and the scattered fields are expressed in terms of characteristic, global reflection, and transmission coefficients. We validated the approach using an ultrawideband frequency domain radar with a transmitting and receiving Vivaldi antenna in the frequency range 0.8–4 GHz. The antenna characteristic coefficients are obtained through a calibration procedure by inversion of near- and far-field measurements with the antenna at different heights over a copper plane. For validating the model, measurements are performed with the antenna at different heights over a water layer with frequency-dependent electrical properties as described by the Debye model to account for relaxation effects. Inversions are performed to estimate the water layer thickness and antenna heights. The proposed radar characterization method, which in particular applies to planar layered media, is presently subject to Patent Application PCT/EP2012/055416 (WO 2012/130847 A1 - "Method and device for characterization of physical properties of a target volume by electromagnetic inspection" by Sébastien Lambot, Université catholique de Louvain, Belgium).

II. Model Formulation

A. Far-Field Model

In the far-field radar model of Lambot *et al.* [18], which applies to planar layered media, a local plane wave field distribution is assumed for the backscattered field over the antenna aperture, and hence, an equivalent single electric dipole approximation holds for describing antenna radiation properties. Relying on the linearity of Maxwell's equations, wave propagation between the point source or field point and the radar transmission line reference plane is accounted for by means of complex, frequency-dependent global reflection and transmission coefficients (see Fig. 1). These characteristic coefficients determine the antenna and transmission line internal transmissions and reflections, and thereby antenna–medium interactions. When the same antenna is simultaneously used as transmitter and receiver, the relation between the radar-measured field and the 3-D layered medium Green's function is described in the frequency domain as follows [18]:

$$S(\omega) = \frac{b(\omega)}{a(\omega)} = R_i(\omega) + \frac{T_{s,1}(\omega)G_{11}(\omega)T_{i,1}(\omega)}{1 - R_{s,1}(\omega)G_{11}(\omega)} \quad (1)$$

where $S(\omega)$ is the radar signal expressed here as the ratio between the backscattered field $b(\omega)$ and incident field $a(\omega)$ at the radar transmission line reference plane, with ω being the angular frequency, $R_i(\omega)$ is the global reflection coefficient of the antenna for fields incident from the radar reference plane onto the source point, corresponding to the free-space antenna response, $T_{s,1}(\omega)$ is the global transmission coefficient for fields incident from the field point onto the radar reference plane, $T_{i,1}(\omega)$ is the global transmission coefficient for fields incident from the radar reference plane onto the source point, and $R_{s,1}(\omega)$ is the global reflection coefficient for fields incident from the layered medium onto the field point. Subscript 1 denotes the index of the source point or field point, which reduces to 1 in the far-field model. The source-field point corresponds to the antenna phase center. The Green's function $G_{..}(\omega)$ is defined as the scattered x-directed electric field $E_{x,.}(\omega)$ at the field point for a unit-strength x-directed electric source $J_{x,.}$ situated at the same location. The Green's function is derived using a recursive scheme to compute the global reflection coefficients of the multilayered medium in the spectral domain [23]–[25]. The transformation back to the spatial domain is performed by evaluating numerically a semi-infinite integral, for which a fast procedure is applied [26]. The spatial-domain Green's function is defined as

$$G_{..} = \frac{1}{8\pi}\int_0^{+\infty} \tilde{G}_{..}(k_\rho)k_\rho dk_\rho \quad (2)$$

where the spectral Green's function is

$$\tilde{G}_{..}(k_\rho) = \left[J_0(k_\rho\rho)\left(\frac{\Gamma_0 R_0^{\mathrm{TM}}}{\sigma_0 + \jmath\omega\varepsilon_0} - \frac{\jmath\omega\mu_0 R_0^{\mathrm{TE}}}{\Gamma_0}\right) - J_2(k_\rho\rho)\cos(2\theta)\left(\frac{\Gamma_0 R_0^{\mathrm{TM}}}{\sigma_0 + \jmath\omega\varepsilon_0} + \frac{\jmath\omega\mu_0 R_0^{\mathrm{TE}}}{\Gamma_0}\right)\right] \times \exp(-2\Gamma_0 h_0). \quad (3)$$

In this expression, J_0 and J_2 are, respectively, the first kind zero- and second-order Bessel's functions, ρ and θ are, respectively, the distance and angle in the xy-plane between the field and source points (referred to by the dots in $G_{..}$, respectively), subscript 0 refers to the upper half-space (free-space), h_0 is the distance between the source/receiver points and the first medium interface, R^{TM} and R^{TE} are, respectively, the transverse magnetic (TM) and transverse electric (TE) global reflection coefficients accounting for all reflections in the multilayered medium, Γ is the vertical wavenumber defined as $\Gamma = \sqrt{k_\rho^2 - k^2}$, while $k^2 = \omega^2\mu(\varepsilon - (\jmath\sigma/\omega))$ with the magnetic permeability μ, dielectric permittivity ε, and electrical conductivity σ. For the free-space layer 0 (upper half-space), we have $k_0^2 = (\omega/c)^2$ with c being the free-space wave velocity. In the far-field expression (1), we consider $\rho = 0$.

B. Near-Field Model

When the layered medium is situated in the near-field of the antenna, the planar field assumption over the antenna aperture

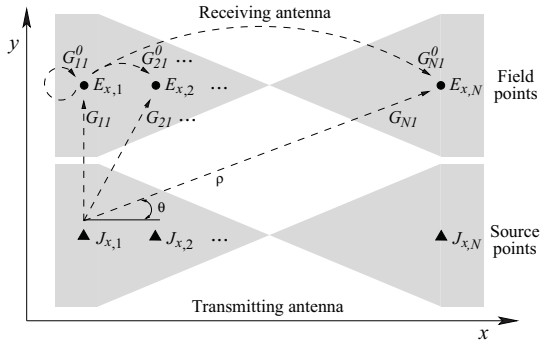

Fig. 2. Distribution of equivalent infinitesimal electric dipole point sources ($J_{x,\cdot}$) and field points ($E_{x,\cdot}$) in the $x-y$ plane of a 3-D Cartesian system for modeling the radar antennas. Gray outlines: bowtie antennas as example to illustrate the interaction paths between antenna sources and the layered medium. Dashed lines: layered medium Green's functions from the sources to the receivers ($G_{\cdot\cdot}$) and from the receivers, acting as secondary sources, to the receivers themselves ($G^0_{\cdot\cdot}$).

does not hold anymore and the scattered field distribution depends on the antenna–medium distance and medium properties. An efficient approach for producing the correct antenna radiation field and capture the scattered field distribution is to consider an equivalent set of infinitesimal electric dipoles ($J_{x,n}$, $n = 1, \ldots, N$) for the source and a set of points ($E_{x,m}$, $m = 1, \ldots, N$) where the field is sampled for the receiver [16], [17], thereby resorting to the superposition principle. Fig. 2 represents an example of such model configuration, showing the infinitesimal electric sources located on a transmitting bowtie antenna and the field points located on the receiving counterpart. When the same antenna is simultaneously used as a transmitter and receiver, the source and field points are the same. The number of points to consider depends on the complexity of the scattered field distribution, which is intrinsically decomposed into a number of elementary distributions, i.e., local plane waves.

As for the far-field model described above, wave propagation between the point sources or field points and the radar transmission line reference plane can be accounted for by means of complex, frequency-dependent global reflection and transmission coefficients. The generalized model is depicted in Fig. 3. Because of the scattered field antenna reflection coefficients, the field points act as well as point sources within infinite reflection loops. Although the part of mutual antenna coupling that depends on the medium is not explicitly included in the proposed model (only free-space coupling is physically described through T_0), it can be shown that it is implicitly accounted for through the linearity of Maxwell's equations. The antenna block diagram shown in Fig. 3 can be solved in a closed form in the frequency domain as the solution of a system of linear equations as follows:

$$S(\omega) = \frac{b(\omega)}{a(\omega)} = T_0(\omega) + \mathbf{T_s}\left(\mathbf{I_N} - \mathbf{G^0 R_s}\right)^{-1}\mathbf{G T_i} \quad (4)$$

with

$$\mathbf{T_i} = \left[T_{i,1}(\omega)\ T_{i,2}(\omega)\ \cdots\ T_{i,N}(\omega)\right]^T \quad (5)$$

$$\mathbf{T_s} = \left[T_{s,1}(\omega)\ T_{s,2}(\omega)\ \cdots\ T_{s,N}(\omega)\right] \quad (6)$$

$$\mathbf{R_s} = \mathrm{diag}\left(\left[R_{s,1}(\omega)\ R_{s,2}(\omega)\ \cdots\ R_{s,N}(\omega)\right]\right) \quad (7)$$

$$\mathbf{G} = \begin{bmatrix} G_{11}(\omega) & G_{12}(\omega) & \cdots & G_{1N}(\omega) \\ G_{21}(\omega) & G_{22}(\omega) & \cdots & G_{2N}(\omega) \\ \vdots & \vdots & & \vdots \\ G_{N1}(\omega) & G_{N2}(\omega) & \cdots & G_{NN}(\omega) \end{bmatrix} \quad (8)$$

and

$$\mathbf{G^0} = \begin{bmatrix} G^0_{11}(\omega) & G^0_{12}(\omega) & \cdots & G^0_{1N}(\omega) \\ G^0_{21}(\omega) & G^0_{22}(\omega) & \cdots & G^0_{2N}(\omega) \\ \vdots & \vdots & & \vdots \\ G^0_{N1}(\omega) & G^0_{N2}(\omega) & \cdots & G^0_{NN}(\omega) \end{bmatrix} \quad (9)$$

where the different quantities are defined as in (1), with $T_0(\omega)$ being the global transmission or reflection coefficient of the antenna in free space (referred to by subscript 0) for nonzero or zero-offset ($T_0(\omega) = R_i(\omega)$) source-receiver, respectively, $G^0_{\cdot\cdot}(\omega)$ being the layered medium Green's functions for fields incident from the field points onto the field points themselves, $\mathbf{I_N}$ being the N-order identity matrix, and superscript T denoting transpose. As the solution of a system of linear equations that solves the block diagram represented in Fig. 3, (4) is expressed. When the number of source and receiver points limits to 1 (far-field, zero-offset configuration), (4) reduces to (1) and the block diagram shown in Fig. 3 reduces to the scheme of Fig. 1.

C. Determination of the Antenna Characteristic Coefficients

The antennas global transmission coefficients $T_0(\omega)$, $T_{i,\cdot}(\omega)$ and $T_{s,\cdot}(\omega)$, and reflection coefficients $R_{s,\cdot}(\omega)$ can be determined by solving (4) for known layered media for which the Green's functions $G_{\cdot\cdot}(\omega)$ and $G^0_{\cdot\cdot}(\omega)$ can be calculated and the corresponding radar measurements $S(\omega)$ can be performed, thereby formulating an inverse problem that can be solved numerically. A practical configuration is to consider near- and far-field measurements with the antenna situated at different heights over a copper plane considered as a perfect electrical conductor. The size of the copper plane should be large enough so that it can be considered as an infinite plane. The antenna calibration inverse problem involves the optimization of a multidimensional objective function, the topography of which is relatively complex and thereby requires a specific optimization strategy that is outlined below.

The proposed optimization scheme is solved independently frequency per frequency and, for one specific frequency, relies on a progressive calibration using radar subdatasets. First, far-field measurements are used to determine the antenna coefficients assuming a single point source and field point [see (1)]. This optimization problem is formulated analytically in a closed form in terms of a system of linear equations [27], [28]. Subsequently, these coefficient values are used as initial guess for the near-field calibration procedure, and in particular, are uniformly distributed over the full set of antenna coefficients pertaining to the complete set of point sources and field points, thereby constituting an initial guess for the complete optimization problem. The initial guess for the transmission functions is $T_{\cdot,\cdot}(\omega) = T^*_{\cdot,1}(\omega)/N$ where $T^*_{\cdot,1}(\omega)$ comes from the far-field model calibration [see (1)] and N represents the number of source/field points. As the incident transmission coefficients $T_{i,n}$ ($n = 1, \ldots, N$) are mathematically fully

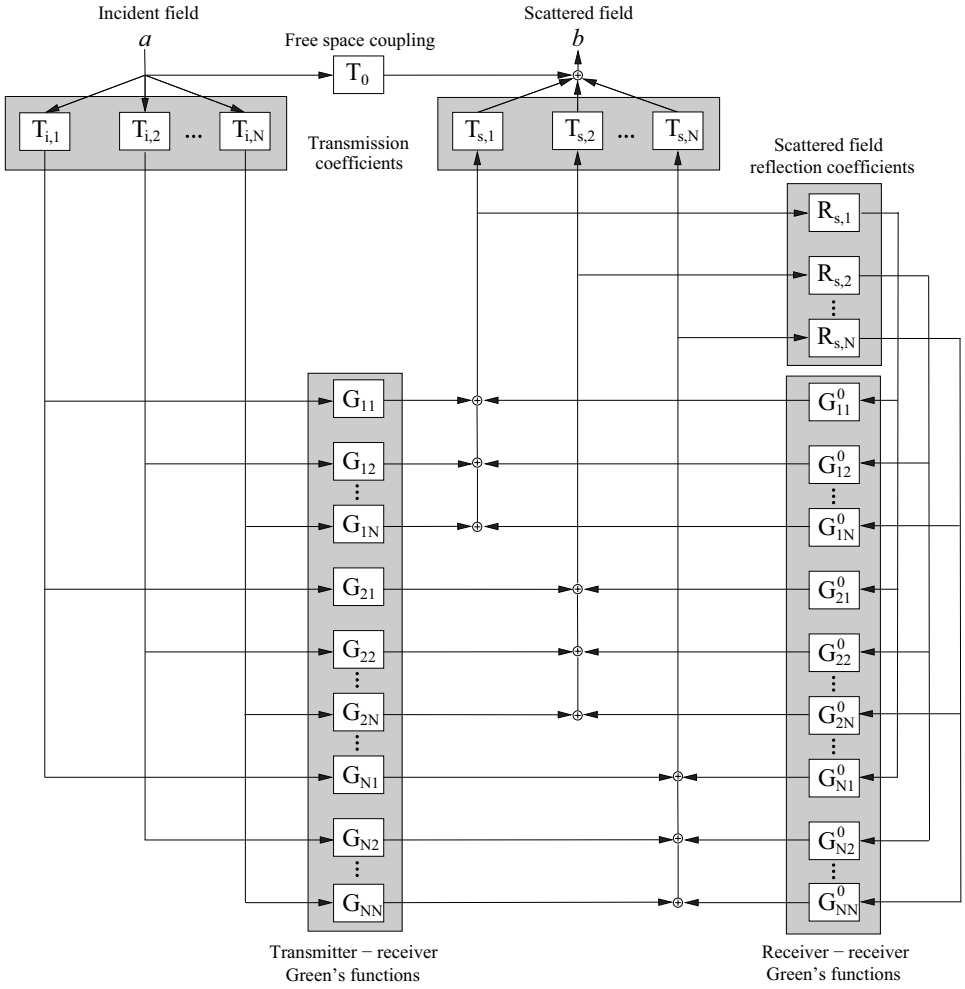

Fig. 3. Linear block diagram representing the transmitting and receiving antenna model where the fields are decomposed into plane waves to which correspond global transmission and reflection coefficients. This block diagram permits to describe wave propagation between the radar reference plane, point sources, and field points.

correlated to their scattering counterpart $T_{s,n}$, only the product $T_{i,n}T_{s,n}$ can be estimated, which thereby reduces the number of unknown functions to determine. It is worth noting that although the $T_0(\omega)$ function is obtained from the far-field calibration, it can also be obtained from a free space measurement. This function is therefore known for the near-field calibration phase. The initial guess for the reflection functions is $R_{s,\cdot}(\omega) = R^*_{s,1}(\omega)$ where $R^*_{s,1}(\omega)$ comes from the far-field model calibration. The symmetry of an antenna can be used to decrease the number of unknowns in the calibration inverse problem.

Once the initial guesses from the far-field calibration are determined, a subset of the near-field radar data pertaining to the highest heights is added to the initial far-field subset and the antenna coefficients are updated using local optimization (e.g., using Levenberg-Marquardt algorithm) to fit (4) to the new radar dataset. The procedure is repeated until the full radar dataset (down to an antenna height of zero) is used. The selection of the radar data subsets should be made such that the optimization algorithm progresses in the correct direction in the parameter space at each iteration. Thus, the height steps should be relatively small with respect to the wavelength to ensure proper convergence of the optimization procedure. The antenna heights should be known with a high level of accuracy, especially relative to each other. When the frequency step in the radar data is sufficiently small, the optimization procedure can be accelerated by using the solution from a previous frequency as initial guess to directly invert the full radar dataset. It is noteworthy that the antenna characteristic coefficients fully describe the antenna and do not depend on the medium. Theoretically, they should only be determined once for a specific transmitting-receiving antenna system.

D. Full-Wave Inversion

The properties of the layered medium can be retrieved by full-wave inversion through which the following objective function, formulated in the least squares sense, is minimized

$$\phi(\mathbf{b}) = \left|\mathbf{S}^* - \mathbf{S}\right|^T \mathbf{C}^{-1} \left|\mathbf{S}^* - \mathbf{S}\right| \tag{10}$$

where $\mathbf{S}^* = S(\omega)$ and $\mathbf{S} = S(\omega, \mathbf{b})$ are the vectors containing, respectively, the observed and simulated radar data, $\mathbf{C}$ is the measurement error covariance matrix, and $\mathbf{b} = [\varepsilon_n, \sigma_n, h_n]$ with $n = 1, \ldots, N$ is the vector of unknowns. The radar data

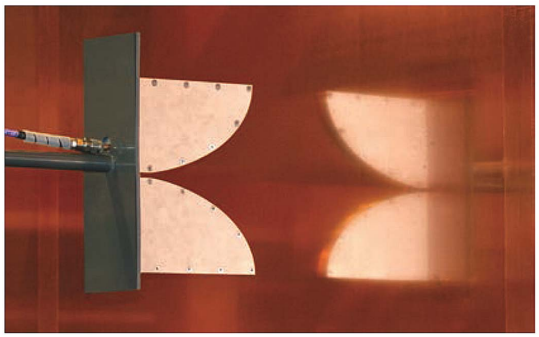

Fig. 4. Picture of the experimental setup for calibrating the Vivaldi antenna by performing measurements at different distances from a copper plane. This homemade antenna was designed by Remy Sarkis and Christophe Craeye (Communications and Remote Sensing Laboratory, UCL).

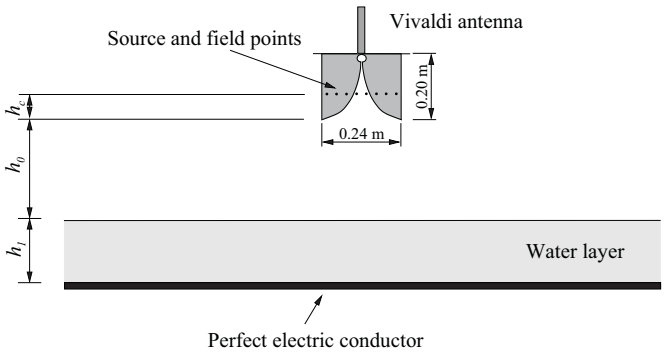

Fig. 5. Sketch of the laboratory experimental setup. The water layer thickness is $h_1 = 0.050$ m, the antenna height above water ranges $h_0 = 0 \cdots 0.760$ m, and the equivalent source and field points were situated at $h_c = 0.075$ m from the antenna aperture and are evenly distributed with 0.03-m spacing.

vectors are arranged versus frequency. Since the radar data are complex valued, the difference between observed and modeled data is expressed by the amplitude of the errors in the complex plane. In this paper, the objective function (10) was minimized using the global multilevel coordinate search algorithm [29] combined sequentially with the classical Nelder-Mead simplex algorithm [30]. Depending on the unknowns to estimate and information content in the radar data, the topography of the objective function to optimize may be relatively complex and the inverse problem may be ill posed. Inversion can be performed equivalently either in the frequency domain or in the time domain, the choice of which depending on an eventual frequency or time filter to apply (see [27]). Inversion in the frequency domain is inherently faster as it avoids the inverse Fourier transform operation.

III. Radar Setup and Model Configuration

The radar is set up using a vector network analyzer (ZVRE, Rohde & Schwarz, Munich, Germany) as stepped-frequency continuous-wave system. A single homemade Vivaldi antenna is used as zero-offset, transmitter, and receiver system (see Fig. 4). The antenna has an aperture of 24 cm and a height of 20 cm. Measurements are performed in the frequency range 0.8–4.0 GHz, with a frequency step of 8 MHz, resulting in 401 different frequencies. We calibrated the vector network analyzer at the connection between the antenna feed point and the coaxial cable using a standard open-short-match calibration kit.

The antenna is modeled using an equivalent set of eight point sources, corresponding as well to the field points given the zero-offset configuration, evenly distributed along a line situated at the far-field phase center height (see Fig. 5). Symmetry of the antenna is assumed, which reduces the number of complex unknowns in the antenna calibration inverse problem. Modeling the antenna using eight points source and receiver, resulting in eight complex unknowns per frequency assuming antenna symmetry, appeared to be an optimal tradeoff between modeling accuracy and modeling computation time (results not shown). The computation time for antenna calibration was about 10 min/frequency using a single 2.83-GHz processor.

IV. Antenna Characteristic Coefficients

To calibrate the Vivaldi antenna, measurements are performed with the antenna at 100 different heights in both the near- and far-fields ($h_0 = 0$–0.76 m) over a 3×3 m^2 copper sheet assumed as a PEC (see Fig. 4). The corresponding Green's functions are calculated and (4) is inverted following the procedure described in Section II-C to calculate the antenna characteristic coefficients. Once these coefficients are known, (4) can be used to simulate the radar data for any layered medium configuration. Fig. 6 shows the measured and modeled radar data, expressed in the time domain [$s(t) = \mathrm{IFFT}(S(\omega))$], over the copper sheet. The antenna internal reflections can be clearly observed at early times as well as the copper sheet reflection that appears at larger times for increasing heights (h_0). A first-order multiple between the antenna and the copper sheet can also be observed. The measured and modeled data agree remarkably well, with differences in terms of signal amplitude that are less than 4% and a correlation coefficient of $r = 0.99934$. The observed errors are not specifically larger in the near-field than in the far-field. They may partly be attributed to the differences between the actual and measured h_0 values and the nonperfect electrical connections between the copper sheets making the full 3×3 m plane.

Fig. 7 shows the amplitude and phase of the global transmission and reflection coefficients as a function of frequency. The T_0 function is estimated from the far-field measurements above the copper plane by inversion of (1). The T_0 function derived in that way closely corresponds, as theoretically expected, to the free space measurement [see Fig. 7(a)]. The function shows a smooth variation with respect to frequency, presenting oscillations in the amplitude that correspond to antenna internal reflections (see the time-domain counterpart at early times in Fig. 6). The amplitude of the transmission coefficient functions $T_{i,\cdot}$ (considered here as the square root of the estimated products $T_{i,\cdot}T_{s,\cdot}$) shows a relatively smooth and oscillating behavior. All four functions have a similar amplitude, showing that all points on the antenna aperture contribute with the same importance to the antenna radiation, depending on frequency. The phase variation with frequency is nearly linear, showing that the antenna is not significantly

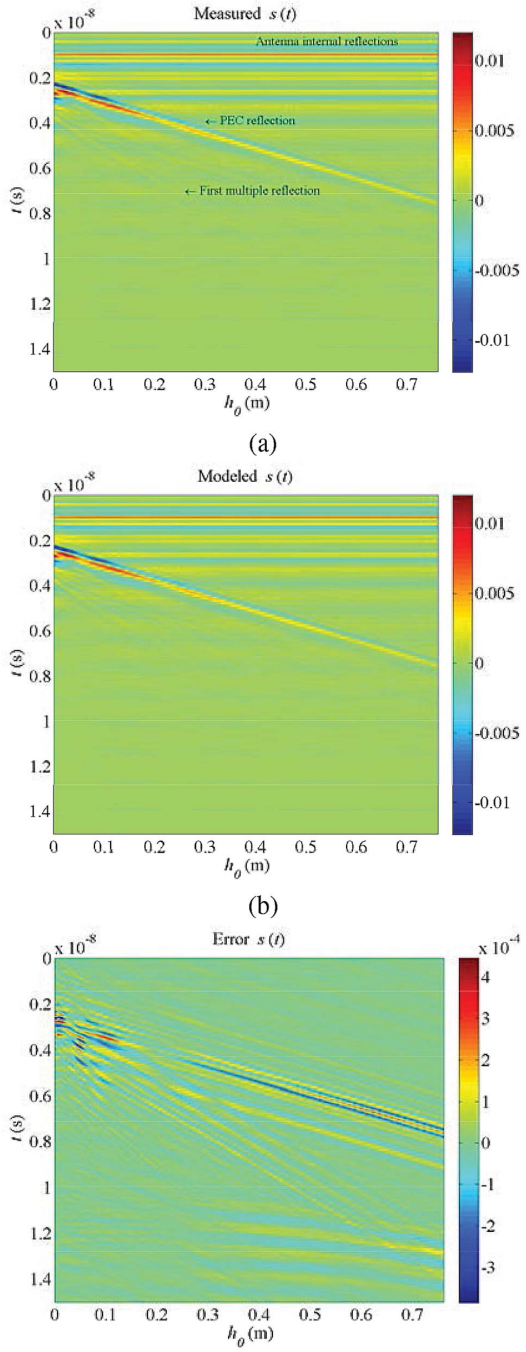

Fig. 6. (a) Measured and (b) modeled radar data expressed in the time domain ($s(t)$) for the antenna at different heights (h_0) over the copper sheet (PEC). (c) Difference between the measured and modeled radar data.

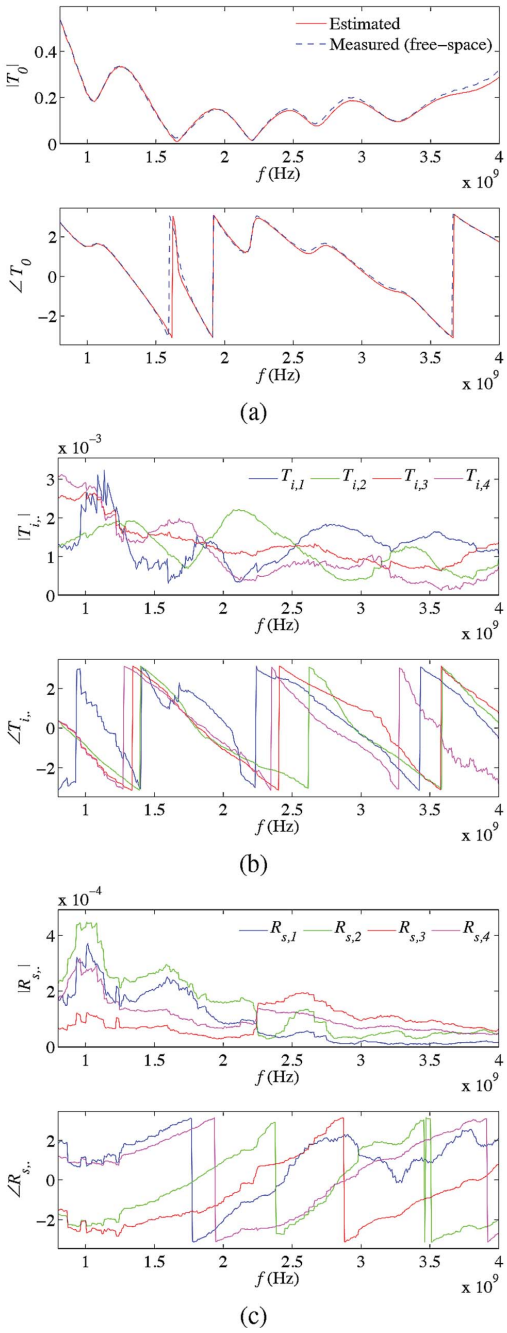

Fig. 7. Amplitude and phase of the characteristic, global transmission (a-b) and reflection (c) coefficients of the Vivaldi antenna as a function of frequency.

dispersive. The global reflection coefficients $R_{s,\cdot}$ also present a relatively smooth behavior, with larger differences between the source and receiver points compared with the transmission functions. The smoothness of all functions strengthens the physical consistency of the calibration as each frequency constitutes an independent calibration problem in this example.

V. Model Validation: Water Measurements

Measurements are performed with the antenna at different heights above a 5-cm-thick and 3 × 3 m area water layer for validating the proposed model (see Fig. 5). A copper plane is used as bottom boundary condition. Water is of particular interest as a validating medium as it is a homogeneous medium with frequency-dependent electrical properties that also depend on salinity and temperature, thereby constituting a well-known medium but with relatively complex properties in that frequency range (0.8–4 GHz). We use the Debye model [31] for describing the frequency dependence of free water electrical properties with parameterizations as provided by [32] and [33] for the complex permittivity values and relaxation time. The water temperature is 17.2 °C and its

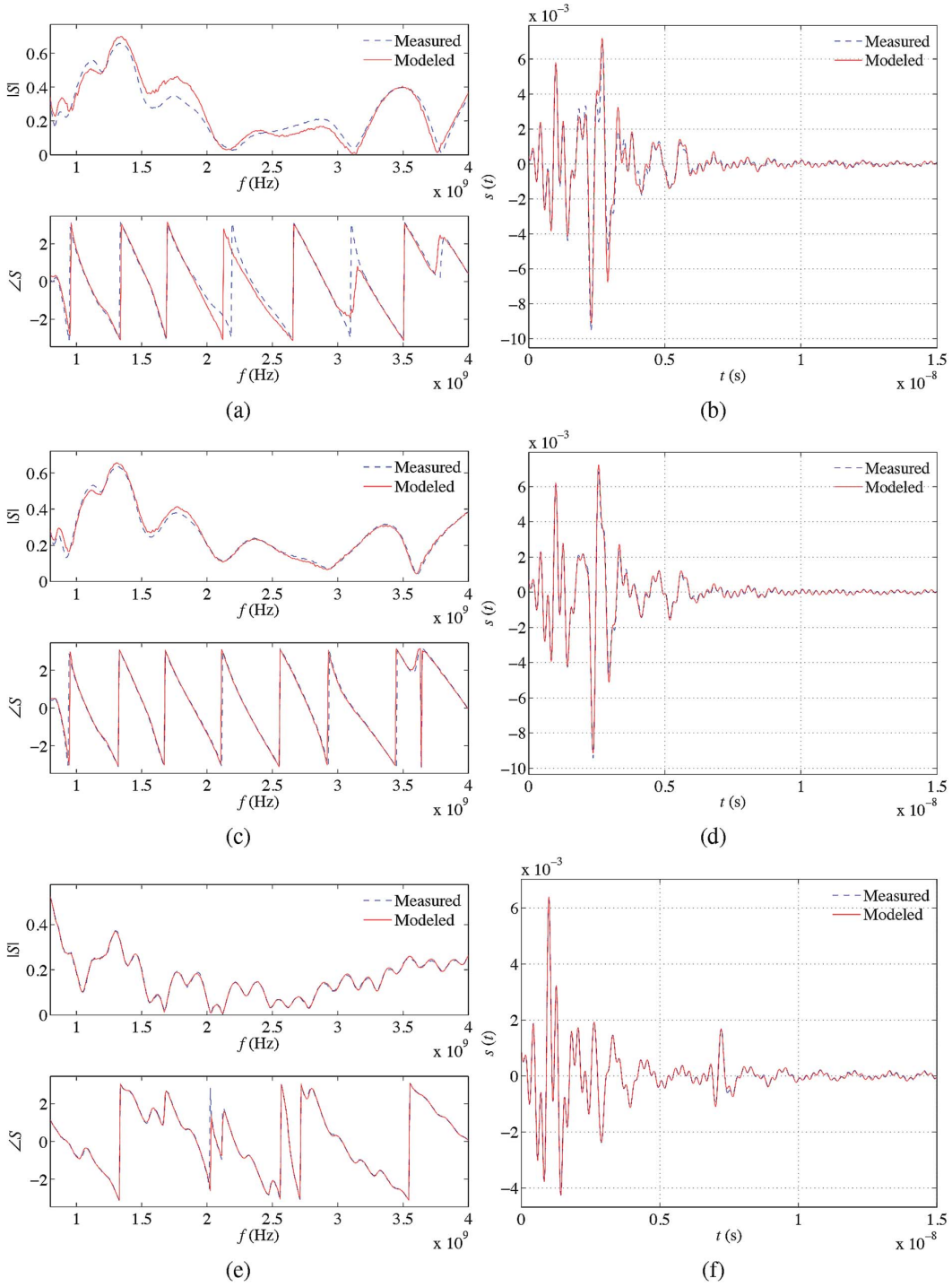

Fig. 8. Measured and modeled radar data in both the (a) frequency and (b) time domains with the antenna aperture situated at 0.00, (c) and (d) 9.86, and (e) and (f) 710.00 mm above the water layer.

dc electrical conductivity is 0.0806 S/m. The computation time for a forward run of the near-field model is about 1–3 s for the 401 frequencies using a single 2.83-GHz processor. The computation time depends on the particular model configurations.

Fig. 8 shows, in both the frequency and time domains, the measured and modeled radar data for measurements collected with the antenna at three different heights (0.00, 9.86, and 710.00 mm) above the water layer. The modeled data are obtained by model inversion with only the water thickness and antenna height as unknowns. Other parameters are fixed to their theoretical value as described above. For all heights, a remarkably high accuracy is achieved by the model to describe the measurements, especially for heights larger than around 10 mm. For $h_0 = 0$ mm, some differences can be observed. These may be attributed to the high sensitivity of the

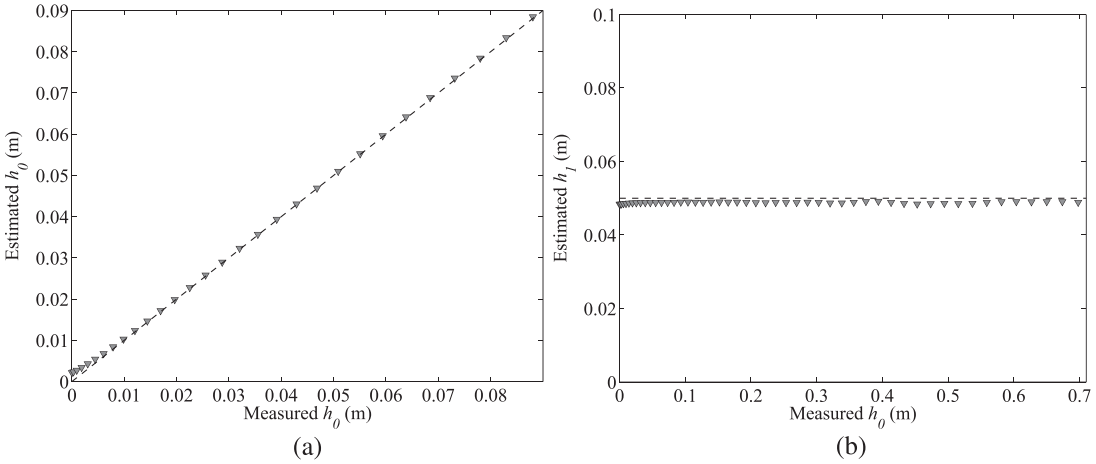

Fig. 9. (a) Inversely estimated antenna height (h_0) and (b) water layer thickness (h_1) with respect to the antenna height above water.

measurements with respect to height in this short range and the limited accuracy in height measurement (around 1 mm) achieved with the present experimental setup. For the largest heights, the reflection at the surface of the water is well decoupled from the antenna internal reflections and antenna–medium coupling and appears around 7 ns. For other heights, the water surface reflection is also visible, but mixed together with the antenna internal reflections and antenna–medium coupling. The copper sheet is expected to be visible around 3 ns after the water surface reflection, but it cannot be discerned from the antenna interferences in that short range because of the multiple reflections as well as wave attenuation within water.

Fig. 9 shows the inverted antenna heights h_0 and water layer thickness h_1 as a function of the actual antenna heights (measured). For all antenna heights, inversions permitted to properly retrieve actual heights. Some discrepancies can be observed, especially for lower antenna heights, which may be attributed to both a possible decreased sensitivity in the inversion process (antenna internal reflections and medium reflections are coupled) and larger modeling errors. In general, the inversion accuracy in terms of height is comparable to the accuracy for the measurement of the actual heights (< 1 mm).

VI. Conclusion

We proposed a novel closed-form equation for modeling near-field radar measurements over planar layered media, which included in particular the antenna effects and its interactions with the medium. The model relied on a plane wave decomposition and global transmission and reflection coefficients that are characteristic to the antenna, thereby providing an intrinsic antenna representation and effective way that takes maximum benefit from the linearity of Maxwell's equations for fast computing. A Vivaldi antenna was calibrated using this method and the model showed an unprecedented accuracy to reproduce both near-field and far-field measurements over a water layer bounded by a copper sheet. A major advantage compared with numerical methods is that only minimal information regarding the antenna geometry is required for proper modeling. We referred to Lambot *et al.* [34] for an example of application using a time-domain GPR equipped with bowtie transmitting and receiving antennas. These results showed the great promise for planar material property retrieval through full-wave inversion. Future research will focus on a deeper analysis of the antenna calibration inverse problem, in particular to address more complex antenna systems such as antenna arrays.

References

[1] J. A. Huisman, S. S. Hubbard, J. D. Redman, and A. P. Annan, "Measuring soil water content with ground penetrating radar: A review," *Vadose Zone J.*, vol. 2, no. 4, pp. 476–491, 2003.

[2] S. Lambot, A. Binley, E. Slob, and S. Hubbard, "Ground penetrating radar in hydrogeophysics," *Vadose Zone J.*, vol. 7, no. 1, pp. 137–139, 2008.

[3] E. Slob, M. Sato, and G. Olhoeft, "Surface and borehole ground-penetrating-radar developments," *Geophysics*, vol. 75, no. 5, pp. A103–A120, 2010.

[4] S. Y. Hyun, S. Y. Kim, and Y. S. Kim, "An equivalent feed model for the FDTD analysis of antennas driven through a ground plane by coaxial lines," *IEEE Trans. Antennas Propag.*, vol. 57, no. 1, pp. 161–167, Jan. 2009.

[5] C. Warren and A. Giannopoulos, "Creating finite-difference time-domain models of commecrical ground-penetrating radar antennas using Taguchi's optimization method," *Geophysics*, vol. 76, no. 2, pp. G37–G47, 2011.

[6] G. Meles, S. Greenhalgh, J. van der Kruk, A. Green, and H. Maurer, "Taming the non-linearity problem in GPR full-waveform inversion for high contrast media," *J. Appl. Geophys.*, vol. 73, no. 2, pp. 174–186, 2011.

[7] T. M. Millington, N. J. Cassidy, L. Nuzzo, L. Crocco, F. Soldovieri, and J. K. Pringle, "Interpreting complex, three-dimensional, near-surface GPR surveys: An integrated modelling and inversion approach," *Near Surf. Geophys.*, vol. 9, no. 3, pp. 297–304, 2011.

[8] N. V. Venkatarayalu, Y. B. Gan, R. Lee, and L. W. Li, "Application of hybrid FETD-FDTD method in the modeling and analysis of antennas," *IEEE Trans. Antennas Propag.*, vol. 56, no. 9, pp. 3068–3072, Sep. 2008.

[9] M. M. Ilic, M. Djordjevic, A. Z. Ilic, and B. M. Notaros, "Higher order hybrid FEM-MoM technique for analysis of antennas and scatterers," *IEEE Trans. Antennas Propag.*, vol. 57, no. 5, pp. 1452–1460, May 2009.

[10] C. Craeye, T. Gilles, and X. Dardenne, "Efficient full-wave characterization of arrays of antennas embedded in finite dielectric volumes," *Radio Sci.*, vol. 44, no. 1, p. RS1S90, Feb. 2009.

[11] Y. Chen, S. Yang, S. He, and Z. Nie, "Fast analysis of microstrip antennas over a frequency band using an accurate MoM matrix interpolation technique," *Progr. Electromagn. Res.*, vol. 109, pp. 301–324, May 2010.

[12] M. F. Pantoja, A. G. Yarovoy, A. R. Bretones, and S. G. Garcia, "Time domain analysis of thin-wire antennas over lossy ground using the reflection-coefficient approximation," *Radio Sci.*, vol. 44, no. 6, p. 14, 2009.

[13] T. K. Sarkar and A. Taaghol, "Near-field to near/far-field transformation for arbitrary near-field geometry utilizing an equivalent electric current and MoM," *IEEE Trans. Antennas Propag.*, vol. 47, no. 3, pp. 566–573, Mar. 1999.
[14] Y. Alvarez, F. Las-Heras, and M. R. Pino, "Reconstruction of equivalent currents distribution over arbitrary three-dimensional surfaces based on integral equation algorithms," *IEEE Trans. Antennas Propag.*, vol. 55, no. 12, pp. 3460–3468, Dec. 2007.
[15] C. Craeye and D. Gonzalez-Ovejero, "A review on array mutual coupling analysis," *Radio Sci.*, vol. 46, no. 2, p. 25, 2011.
[16] M. Serhir, P. Besnier, and M. Drissi, "Antenna modeling based on a multiple spherical wave expansion method: Application to an antenna array," *IEEE Trans. Antennas Propag.*, vol. 58, no. 1, pp. 51–58, Jan. 2010.
[17] G. G. Gentili and U. Spagnolini, "Electromagnetic inversion in monostatic ground penetrating radar: TEM horn calibration and application," *IEEE Trans. Geosci. Remote Sens.*, vol. 38, no. 4, pp. 1936–1946, Jul. 2000.
[18] S. Lambot, E. C. Slob, I. van den Bosch, B. Stockbroeckx, and M. Vanclooster, "Modeling of ground-penetrating radar for accurate characterization of subsurface electric properties," *IEEE Trans. Geosci. Remote Sens.*, vol. 42, no. 11, pp. 2555–2568, Nov. 2004.
[19] J. Minet, S. Lambot, E. C. Slob, and M. Vanclooster, "Soil surface water content estimation by full-waveform GPR signal inversion in the presence of thin layers," *IEEE Trans. Geosci. Remote Sens.*, vol. 48, no. 3, pp. 1138–1150, Mar. 2010.
[20] F. Soldovieri, O. Lopera, and S. Lambot, "Combination of advanced inversion techniques for an accurate target localization via GPR for demining applications," *IEEE Trans. Geosci. Remote Sens.*, vol. 49, no. 1, pp. 451–461, Jan. 2011.
[21] C. Patriarca, S. Lambot, M. R. Mahmoudzadeh, J. Minet, and E. Slob, "Reconstruction of sub-wavelength fractures and physical properties of masonry media using full-waveform inversion of proximal penetrating radar," *J. Appl. Geophys.*, vol. 74, no. 1, pp. 26–37, 2011.
[22] D. Moghadas, F. André, H. Vereecken, and S. Lambot, "Efficient loop antenna modeling for zero-offset, off-ground electromagnetic induction in multilayered media," *Geophysics*, vol. 75, no. 4, pp. WA125–WA134, 2010.
[23] W. C. Chew, *Waves and Fields in Inhomogeneous Media*. New York, NY, USA: Van Nostrand, 1990.
[24] K. A. Michalski and J. R. Mosig, "Multilayered media Green's functions in integral equation formulations," *IEEE Trans. Antennas Propag.*, vol. 45, no. 3, pp. 508–519, Mar. 1997.
[25] E. C. Slob and J. Fokkema, "Coupling effects of two electric dipoles on an interface," *Radio Sci.*, vol. 37, no. 5, p. 1073, 2002.
[26] S. Lambot, E. Slob, and H. Vereecken, "Fast evaluation of zero-offset Green's function for layered media with application to ground-penetrating radar," *Geophys. Res. Lett.*, vol. 34, no. 21, p. L21405, 2007.
[27] S. Lambot, L. Weihermüller, J. A. Huisman, H. Vereecken, M. Vanclooster, and E. C. Slob, "Analysis of air-launched ground-penetrating radar techniques to measure the soil surface water content," *Water Resour. Res.*, vol. 42, no. 11, pp. W11403, 2006.
[28] K. Z. Jadoon, S. Lambot, E. C. Slob, and H. Vereecken, "Analysis of horn antenna transfer functions and phase-center position for modeling off-ground GPR," *IEEE Trans. Geosci. Remote Sens.*, vol. 49, no. 5, pp. 1649–1662, May 2011.
[29] W. Huyer and A. Neumaier, "Global optimization by multilevel coordinate search," *J. Global Optim.*, vol. 14, no. 4, pp. 331–355, 1999.
[30] J. C. Lagarias, J. A. Reeds, M. H. Wright, and P. E. Wright, "Convergence properties of the Nelder–Mead simplex method in low dimensions," *SIAM J. Optim.*, vol. 9, no. 1, pp. 112–147, 1998.
[31] P. Debye, *Polar Molecules*. New York, NY, USA: Reinhold, 1929.
[32] A. Stogryn, "Brightness temperature of a vertically structured medium," *Radio Sci.*, vol. 5, no. 12, pp. 1397–1406, 1970.
[33] L. Klein and C. Swift, "Improved model for dielectric-constant of sea-water at microwave-frequencies," *IEEE Trans. Antennas Propag.*, vol. 25, no. 1, pp. 104–111, Jan. 1977.
[34] S. Lambot, F. André, E. Slob, and H. Vereecken, "Effect of antenna-medium coupling in the analysis of ground-penetrating radar data," *Near Surf. Geophys.*, vol. 10, no. 6, pp. 631–639, 2012.

Sébastien Lambot received the M.Sc. and Ph.D. degrees in agricultural and environmental engineering from the Université Catholique de Louvain (UCL), Louvain-La-Neuve, Belgium, in 1999 and 2003, respectively.

He was with the Delft University of Technology, Delft, The Netherlands, from 2004 to 2005, as a European Marie-Curie Post-doctoral Scientist. From 2006 to 2012, he was with Forschungszentrum Jülich, Jülich, Germany, as a Research Group Leader. Since 2006, he has been a Professor and Fonds de la Recherche Scientifique (FNRS) Researcher at UCL. His current research interests include hydrogeophysics and ground-penetrating radar and electromagnetic induction forward and inverse modeling for the remote characterization of soil and material properties.

Dr. Lambot was the General Chair of the 3rd International Workshop on Advanced Ground Penetrating Radar in 2005 and is organizing the 15th International Conference on Ground Penetrating Radar in 2014. He is an Associate Editor for the *Vadose Zone Journal*.

Frédéric André received the M.Sc. and Ph.D. degrees in agricultural and environmental engineering from the Université Catholique de Louvain (UCL), Louvain-La-Neuve, Belgium, in 1999 and 2007, respectively.

He was with the Forschungszentrum Jülich, Jülich, Germany, as a Post-doctoral Scientist, from 2008 to 2011. Since 2011, he has been a FNRS Researcher at UCL. His current research interests include forest sciences and ground-penetrating radar and electromagnetic induction data processing for digital soil mapping.

Dr. André is co-organizing the 15th International Conference on Ground Penetrating Radar (2014).